Collider probes of four-lepton final states in maximally flavor-violating $U(1)_{L_\mu - L_\tau}$ model*

Jianing Qin (秦嘉宁)[1] Fei Huang (黄飞)[1†] Honglei Li (李洪蕾)[1‡] Zhi-Long Han (韩志龙)[1§] Jin Sun (孙进)[2¶]

[1]School of Physics and Technology, University of Jinan, Jinan, Shandong 250022, China
[2]Particle Theory and Cosmology Group, Center for Theoretical Physics of the Universe, Institute for Basic Science (IBS), Daejeon 34126, Korea

Abstract: We investigate the collider signatures of a maximally flavor-violating $U(1)_{L_\mu - L_\tau}$ model, where a new gauge boson Z' and scalar triplets induce lepton flavor-changing interactions in the μ-τ sector. Focusing on four-lepton final states at multi-TeV lepton colliders, we conduct a detailed analysis of cross sections, asymmetries, and polarization effects. We show that the signal cross section is highly sensitive to $m_{Z'}$ and the effective parameters $\tilde{g}/m_{Z'}$, whereas it remains largely insensitive to the triplet Yukawa couplings within the phenomenologically allowed region. The forward-backward asymmetry exhibits a characteristic monotonic dependence on $m_{Z'}$, and beam polarization can significantly suppress the Standard Model backgrounds while enhancing new physics contributions. We find that, in the phenomenologically allowed parameter space, the predicted observables remain highly sensitive to the underlying model parameters. These results show that multi-lepton final states are powerful probes of the $U(1)_{L\mu - L_\tau}$ framework and can offer valuable guidance for future searches at muon and electron-positron colliders.

Keywords: flavor changing processes, lepton collider, new gauge boson Z', triplet Higgs

DOI: 10.1088/1674-1137/ae2b5e **CSTR:** 32044.14.ChinesePhysicsC.50043101

I. INTRODUCTION

The Standard Model (SM) of particle physics successfully describes all known elementary particles and their interactions [1]. However, the observation of neutrino oscillations suggests that neutrinos possess nonzero masses and that neutral lepton flavor violation (LFV) occurs, thereby strongly indicating the potential for charged LFV. Within the SM, charged LFV processes arise only at the loop level and are highly suppressed because neutrino masses are much smaller compared to masses at the electroweak scale, with branching ratios such as $\mathrm{Br}(\mu \to e\gamma) \sim 10^{-55}$ [2, 3]. Consequently, the predicted rates of LFV processes within the SM lie far below current and foreseeable experimental sensitivity. Therefore, any observable LFV signal would constitute compelling evidence for physics beyond the SM.

Numerous extensions of the SM predict observable charged LFV, including supersymmetric models [2, 4, 5], left-right symmetric frameworks [6−10], seesaw mechanisms [11−14], leptoquark scenarios [15−18], Goldstone scenarios [19, 20], and Z' models [21−25], each providing distinct sources and characteristic signatures of flavor violation. Among these, the anomaly-free $U(1)_{L_\mu - L_\tau}$ gauge symmetry model is particularly compelling, as it naturally explains the flavor structure of the lepton sector [26−32]. In this study, we investigated a maximally flavor-violating realization of the $U(1)_{L_\mu - L_\tau}$ model, which permits sizable LFV couplings and leads to distinctive multilepton signatures at colliders. This framework is realized by introducing off-diagonal gauge interactions and new scalar fields that break the flavor symmetry in a controlled manner [33]. As a result, the associated Z' boson and extended Higgs sector can mediate LFV processes at tree level, thereby significantly enhancing the prospects for observing such signals. Furthermore, the model remains consistent with existing constraints from precision electroweak measurements, neutrino oscillation

Received 19 September 2025; Accepted 10 December 2025; Accepted manuscript online 11 December 2025

* Supported by National Natural Science Foundation of China (12505112, 11805081), Shandong Province Natural Science Foundation (ZR2024QA138, ZR2022MA056) and State Key Laboratory of Dark Matter Physics, University of Jinan Disciplinary Cross-Convergence Construction Project 2024 (XKJC- 202404) and Jin Sun is supported by IBS under the project code, (IBS-R018-D1)

† E-mail: sps_huangf@ujn.edu.cn
‡ E-mail: sps_lihl@ujn.edu.cn
§ E-mail: sps_hanzl@ujn.edu.cn
¶ E-mail: sunjin0810@ibs.re.kr

Content from this work may be used under the terms of the Creative Commons Attribution 3.0 licence. Any further distribution of this work must maintain attribution to the author(s) and the title of the work, journal citation and DOI. Article funded by SCOAP[3] and published under licence by Chinese Physical Society and the Institute of High Energy Physics of the Chinese Academy of Sciences and the Institute of Modern Physics of the Chinese Academy of Sciences and IOP Publishing Ltd

data, and rare decay searches, provided that the Z' mass and coupling strengths are appropriately chosen. Notably, sizable LFV couplings are allowed without violating current experimental limits, particularly in the μ-τ sector, which is significantly less constrained than the e-μ and e-τ channels [34].

Lepton colliders offer a clean experimental environment with well-defined initial states, thereby making them ideal for precision electroweak measurements and the search for rare or forbidden phenomena such as LFV [35−42]. In particular, future high-luminosity electron-positron colliders —such as the CLIC [43], ILC [44], CEPC [45, 46], and FCC-ee [47]—can provide excellent sensitivity to multilepton final states, owing to their low background levels and high lepton detection efficiencies. These facilities enable detailed reconstruction of kinematic distributions and invariant mass spectra, thereby facilitating resonance searches for new particles such as the Z' boson. Within the framework of the $U(1)_{L_\mu-L_\tau}$ model with maximal LFV, the observation of final states involving mixed lepton flavors [48] constitutes a smoking-gun signature of new physics. Moreover, advanced flavor-tagging techniques and high energy resolution enable the disentanglement of various decay modes and a detailed study of the underlying LFV couplings. In addition to electron-positron colliders, muon colliders have recently attracted significant attention as promising next-generation facilities. With the potential to achieve multi-TeV center-of-mass energies and deliver high luminosity, muon colliders offer powerful probes for both flavor-conserving and flavor-violating new physics [49]. Their unique initial state allows for the direct production of particles that couple to muons, such as the Z' boson in the $U(1)_{L_\mu-L_\tau}$ model [40]. Correspondingly, a large muon coupling enhances the sensitivity to interactions involving second- and third-generation leptons, which makes muon colliders particularly well-suited for probing LFV in the μ-τ sector.

In this study, we focused on four-lepton final states as clean and sensitive probes of LFV. The structure of the rest of the paper is as follows. In Section II, we present the construction of the maximally flavor-violating $U(1)_{L_\mu-L_\tau}$ model, where Z' interactions are augmented by triplet scalar fields. In Section III, we discuss the analysis of the resulting collider signatures, with a focus on four-lepton final states at both muon and electron-positron colliders. Finally, we summarize our findings and offer concluding remarks in Section IV.

II. $U(1)_{L_\mu-L_\tau}$ MODEL FOR MAXIMAL $\mu-\tau$ COUPLING

$U(1)_{L_\mu-L_\tau}$ gauge symmetry corresponds to the difference between the muon and tau lepton numbers. In the minimal setup, the left-handed doublets, $L_{Li}:(1,2,-1/2)$, and right-handed singlets, $e_{Ri}:(1,1,-1)$, transform under the gauged $U(1)_{L_\mu-L_\tau}$ symmetry, with charges 0, +1, and −1 assigned to the first, second, and third generations, respectively. Here, the numbers in parentheses denote the quantum numbers under the $SU(3)_C\times SU(2)_L\times U(1)_Y$ gauge group. The Z' gauge boson in this model couples exclusively to leptons in the weak interaction basis [26, 27] as follows:

$$\mathcal{L}_{Z'} = -\tilde{g}(\bar{\mu}\gamma^\mu\mu - \bar{\tau}\gamma^\mu\tau + \bar{\nu}_\mu\gamma^\mu L\nu_\mu - \bar{\nu}_\tau\gamma^\mu L\nu_\tau)Z'_\mu\,, \tag{1}$$

where $\tilde{g}$ is the gauge coupling associated with the $U(1)_{L\mu-L_\tau}$ symmetry. L/R denotes the chiral projection $P_{L/R}=(1\mp\gamma_5)/2$. The vector current interaction positively contributes to the muon anomalous magnetic moment $(g-2)_\mu$. The $U(1)_{L_\mu-L_\tau}$ symmetry is spontaneously broken owing to introduction of a singlet scalar field S with charge +1 and vacuum expectation value (VEV) of $v_S/\sqrt{2}$, using which the Z' boson acquires a mass given by $m_{Z'}=\tilde{g}v_S$.

The interaction described above is purely flavor-conserving but can be extended to incorporate flavor-changing effects. We briefly outline the construction of such a model below. This extension requires the introduction of three Higgs doublets $H_{1,2,3}:(1,2,1/2)$ with VEVs $\langle H_i\rangle = v_i/\sqrt{2}$ and $U(1)_{L_\mu-L_\tau}$ charges 0, +2, and −2, respectively. An unbroken exchange symmetry is imposed under which $Z'\to -Z'$, $H_1\leftrightarrow H_1$, and $H_2\leftrightarrow H_3$, with $v_2=v_3\equiv v$. Under these conditions, the Z' interactions and lepton Yukawa couplings are given by

$$\begin{aligned}\mathcal{L}_H = &-\tilde{g}(\bar{l}_2\gamma^\mu Ll_2 - \bar{l}_3\gamma^\mu Ll_3 + \bar{e}_2\gamma^\mu Re_2 - \bar{e}_3\gamma^\mu Re_3)Z'_\mu\\ &-[Y^l_{11}\bar{l}_1Re_1 + Y^l_{22}(\bar{l}_2Re_2+\bar{l}_3Re_3)]H_1\\ &-Y^l_{23}(\bar{l}_2Re_3H_2+\bar{l}_3Re_2H_3)+\text{H.C.}\end{aligned} \tag{2}$$

After electroweak symmetry breaking, the scalar fields acquire non-zero VEVs, which generate charged lepton masses via the Yukawa interactions, which are expressed in the second line of Eq. (2). However, becaue the resulting mass matrix is not diagonal, it must be diagonalized using the following transformation:

$$\begin{pmatrix}\mu\\ \tau\end{pmatrix} = \frac{1}{\sqrt{2}}\begin{pmatrix}1 & -1\\ 1 & 1\end{pmatrix}\begin{pmatrix}e_2\\ e_3\end{pmatrix}. \tag{3}$$

A similar transformation is also applied to the neutrino sector. After rotating to the charged lepton mass eigenstate basis using the above transformation, the desired flavor-changing Z' interactions take the following form:

$$\mathcal{L}_{Z'} = -\tilde{g}(\bar{\mu}\gamma^\mu\tau + \bar{\tau}\gamma^\mu\mu + \bar{\nu}_\mu\gamma^\mu L\nu_\tau + \bar{\nu}_\tau\gamma^\mu L\nu_\mu)Z'_\mu\,. \tag{4}$$

The aforementioned Z' interaction significantly enhances the branching ratio of the process $\tau \to \mu \bar{\nu}_\mu \nu_\tau$. This effect can be alleviated by introducing three scalar triplets with hypercharge $Y = 1$, $\Delta_{1,2,3} : (1,3,1)$, each acquiring VEVs $\langle \Delta_i \rangle = v_{\Delta_i}/\sqrt{2}$ and carrying $U(1)_{L_\mu - L_\tau}$ charges of 0, −2, and +2, respectively [23]. The Δ fields form the core of the well-known type-II seesaw mechanism, which generates small neutrino masses [50−55] with

$$\Delta = \begin{pmatrix} \Delta^+/\sqrt{2} & \Delta^{++} \\ \Delta^0 & -\Delta^+/\sqrt{2} \end{pmatrix}, \quad \Delta^0 = \frac{v_\Delta + \delta + i\eta}{\sqrt{2}}. \tag{5}$$

Under the above exchange symmetry $\Delta_1 \leftrightarrow \Delta_1$, $\Delta_2 \leftrightarrow \Delta_3$ with $v_{\Delta_2} = v_{\Delta_3}$, we use the transformation given in Eq. (3) to express the Yukawa terms in terms of the component fields Δ^0, Δ^+, and Δ^{++} as

$$\mathcal{L}_\Delta = -(\bar{\nu}_e^c, \bar{\nu}_\mu^c, \bar{\nu}_\tau^c) M(\Delta^0) L \begin{pmatrix} \nu_e \\ \nu_\mu \\ \nu_\tau \end{pmatrix} + \sqrt{2}(\bar{\nu}_e^c, \bar{\nu}_\mu^c, \bar{\nu}_\tau^c) M(\Delta^+) L \begin{pmatrix} e \\ \mu \\ \tau \end{pmatrix} + (\bar{e}^c, \bar{\mu}^c, \bar{\tau}^c) M(\Delta^{++}) L \begin{pmatrix} e \\ \mu \\ \tau \end{pmatrix},$$
$$\text{with} \quad M(\Delta) = \begin{pmatrix} Y^\nu_{11}\Delta_1 & 0 & 0 \\ 0 & (Y^\nu_{22}(\Delta_2+\Delta_3) - 2Y^\nu_{23}\Delta_1)/2 & Y^\nu_{22}(\Delta_2 - \Delta_3)/2 \\ 0 & Y^\nu_{22}(\Delta_2 - \Delta_3)/2 & (Y^\nu_{22}(\Delta_2+\Delta_3) + 2Y^\nu_{23}\Delta_1)/2 \end{pmatrix}. \tag{6}$$

We find that the large number of model parameters makes the analysis complex. For simplicity, we adopt the following assumptions.

- $m_{\Delta^{++,+,0}} = m_\Delta$: Degeneracy of the triplet components guarantees that the triplet scalars possess identical masses, which is a requirement that demands $m_\Delta > 420$ GeV [56] for $v_\Delta \sim O(1)$ GeV.

- $Y_{11,23} << Y_{22}$: This suppresses the effects of Δ_1, resulting in triplet contributions dominated by Δ_2 and Δ_3.

- $\Delta_2 \sim \Delta_3$: Off-diagonal interactions are forbidden by the exact exchange symmetry, which may be broken by quantum corrections at the two-loop level. Therefore, we consider the case where the diagonal coupling is approximately ten orders of magnitude larger than the off-diagonal coupling.

The above assumptions ensure that the triplet effects can be effectively described solely by the Δ_2 parameters as follows:

$$\mathcal{L}_{\Delta_2} = \Delta_2^{++}(\bar{\mu}^c, \bar{\tau}^c) \begin{pmatrix} y_{22} & y_{23} \\ y_{23} & y_{22} \end{pmatrix} L \begin{pmatrix} \mu \\ \tau \end{pmatrix}, \quad y_{22}/y_{23} = 10. \tag{7}$$

In the following collider analysis, we employ the above couplings to perform a study with the subscript "2" omitted.

III. ANALYSIS OF FOUR-BODY DECAY RESULTS AT LEPTON COLLIDERS

Before presenting the detailed collider analysis, we first discuss the current existing bounds on the model parameters.

- $(g-2)_l$: One-loop exchanges of Z' and $\Delta^{+,++}$ contribute to muon $(g-2)_\mu$, with opposite contributions as [23, 24]

$$\Delta a_\mu = \Delta a_\mu^{Z'} + \Delta a_\mu^{\Delta} = \frac{\tilde{g}^2_{Z'} m_\mu^2}{12\pi^2 m^2_{Z'}} \left(\frac{3m_\tau}{m_\mu} - 2 \right) - \frac{m_\mu^2}{16\pi^2} \frac{y_{22}^2}{m_\Delta^2}. \tag{8}$$

Here, we adopt the limit $m_{\Delta,Z'} >> m_{\tau,\mu}$. For $(g-2)_\mu$, FNAL reported a new experimental world average [57], which, together with the updated theoretical prediction using lattice QCD calculations alone [58], yields a deviation of $a_\mu^{\rm exp} - a_\mu^{\rm SM} = 39(64) \times 10^{-11}$. Furthermore, the opposite contributions from Z' and Δ cancel each other out, resulting in consistency with the recent muon $(g-2)_\mu$ measurement. A 2σ confidence level is applied to constrain the model parameters in the $\epsilon - m_{Z'}$ plane, as indicated in blue in Fig. 1.

- $\tau \to \mu\nu\bar{\nu}$: The decay processes are mediated by Z' and Δ^+ effects in terms of the ratios as [23, 24]

$$R^\tau \equiv \frac{\Gamma(\tau^- \to \mu^- \bar{\nu}_\mu \nu_\tau)}{\Gamma(\tau^- \to \mu^- \bar{\nu}_\mu \nu_\tau)_{\rm SM}} = \left(1 - \frac{4m_W^2}{g^2} \frac{y_{22}^2}{4m^2_{\Delta^+}} \right)^2$$

$$+\frac{4m_W^2}{g^2}\frac{\tilde{g}^2}{m_{Z'}^2}\left(1-\frac{4m_W^2}{g^2}\frac{y_{22}^2}{4m_{\Delta^+}^2}\right)+\frac{\tilde{g}^4}{g^4}\frac{4m_W^4}{m_{Z'}^4}\,. \tag{9}$$

Combining the SM predictions $R^{\tau}_{\rm SM}=0.972564\pm0.00001$ [59] and average experimental values $R^{\tau}_{\rm aver}=0.972968\pm0.002233$ from the HFLAV collaboration [60] and Belle-II [61], the ratio can be obtained as $R^{\tau}=1.00042\pm0.00230$, which imposes stringent bounds as shown in Fig. 1.

- $\nu_\mu+N\to\nu_{\mu,\tau}+N+\mu^+\mu^-$: The neutrino trident process is induced by Δ^+ at tree-level as [23, 24]

$$\frac{\sigma_{\Delta^+}}{\sigma_{\rm SM}}\Big|_{\rm trident}=\frac{\left(1+4s_W^2-\frac{m_W^2}{g^2}\frac{2y_{22}^2}{m_\Delta^2}\right)^2+\left(1-\frac{m_W^2}{g^2}\frac{2y_{22}^2}{m_\Delta^2}\right)^2}{[(1+4s_W^2)^2+1]}\,, \tag{10}$$

Combining the current bounds from CHARM, CCFR, and NuTeV [62–64], we obtained the averaged value 0.95 ± 0.25.

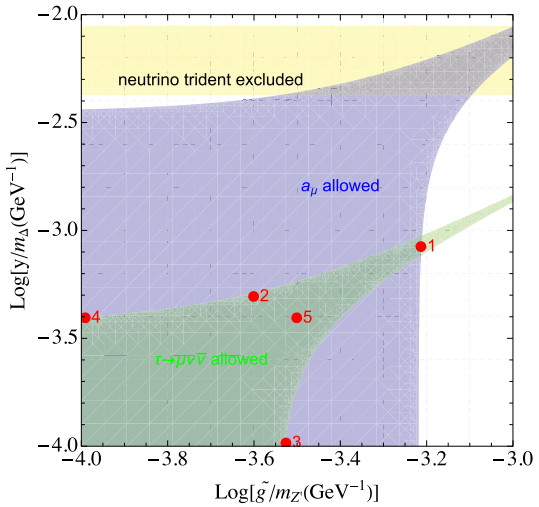

Fig. 1. (color online) Allowed model parameter spaces in the $\tilde{g}/m_{Z'}$-y/m_Δ plane. Different constraints are indicated using distinct colors: green for $\tau\to\mu\nu\bar{\nu}$, yellow for the neutrino trident process, and blue for muon $(g-2)$. Here, red markers denote the selected benchmark points, chosen to represent typical and extreme parameter ratios of the Z' boson and triplet scalars.

Motivated by the aforementioned constraints, we explore the viable parameter space of the $U(1)_{L_\mu-L_\tau}$ model as a potential explanation for the observed deviations in Fig. 1. In order to better visualize the relevance between the lepton collider sensitivity and allowed regions, we define several benchmark points as follows:

$$\begin{aligned}
B1:&\tilde{g}/m_{Z'}({\rm GeV}^{-1})=0.62\times10^{-3}\,,\\
&y/m_\Delta({\rm GeV}^{-1})=0.83\times10^{-3}\,,\\
B2:&\tilde{g}/m_{Z'}({\rm GeV}^{-1})=0.25\times10^{-3}\,,\\
&y/m_\Delta({\rm GeV}^{-1})=0.5\times10^{-3}\,,\\
B3:&\tilde{g}/m_{Z'}({\rm GeV}^{-1})=0.3\times10^{-3}\,,\\
&y/m_\Delta({\rm GeV}^{-1})=0.1\times10^{-3}\,,\\
B4:&\tilde{g}/m_{Z'}({\rm GeV}^{-1})=0.1\times10^{-3}\,,\\
&y/m_\Delta({\rm GeV}^{-1})=0.4\times10^{-3}\,,\\
B5:&\tilde{g}/m_{Z'}({\rm GeV}^{-1})=0.32\times10^{-3}\,,\\
&y/m_\Delta({\rm GeV}^{-1})=0.4\times10^{-3}\,.
\end{aligned} \tag{11}$$

These benchmarks exhibit varied combinations of the gauge parameter $\tilde{g}/m_{Z'}$ and triplet scalar parameter y/m_Δ, thereby ensuring both phenomenological viability and distinctive collider signatures.

A. Four-body final states at the muon colliders

In the maximally flavor-violating model $U(1)_{L_\mu-L_\tau}$, the process $\mu^-\mu^+\to\mu^\pm\mu^\mp+\tau^\pm\tau^\mp$ can be mediated by the gauge boson Z' and new Higgs scalars, as shown in the typical Feynman diagram in Fig. 2.

For the benchmark points mentioned above, we calculate the production cross sections $\sigma(\mu^-\mu^+\to\mu^\pm\mu^\mp+\tau^\pm\tau^\mp)$ as a function of $m_{Z'}$ at the muon collider, as presented in the left panel of Fig. 3. We find that the corresponding cross sections increase monotonically with $m_{Z'}$, thereby reflecting the enhanced phase space and coupling strengths at higher resonance masses. Benchmark B1 yields the largest cross sections, reaching 10^{-3} pb for

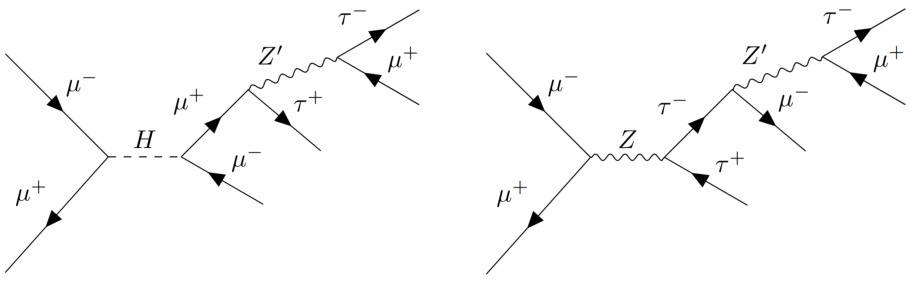

Fig. 2. Representative Feynman diagrams for the four-lepton processes.

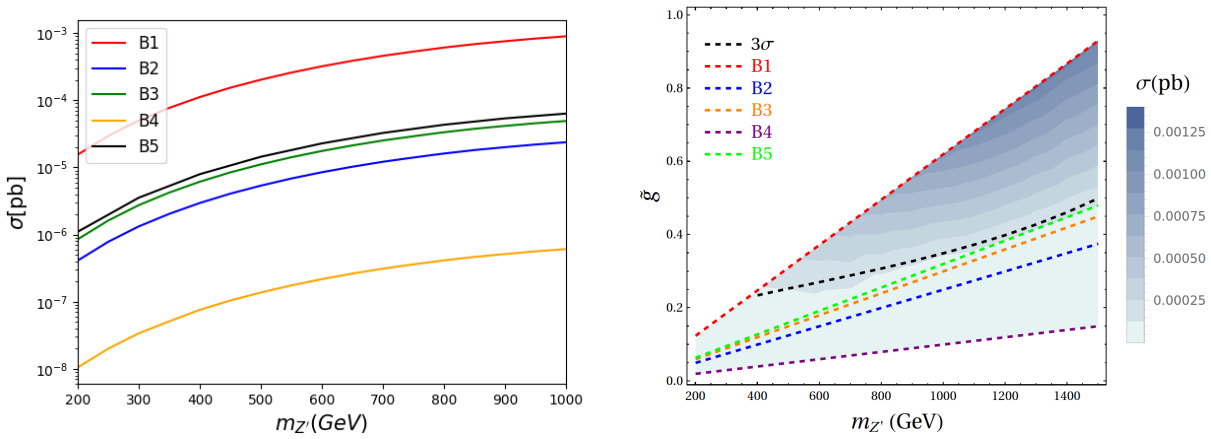

Fig. 3. (color online) (a) Cross section $\sigma(\mu^-\mu^+ \to \mu^\pm\mu^\mp + \tau^\pm\tau^\mp)$ as a function of $m_{Z'}$ at the muon collider with $\sqrt{s} = 3$ TeV. (b) Signal cross-section in the plane $\tilde{g} - m_{Z'}$.

$m_{Z'} \sim 1$ TeV. In contrast, B4 predicts significantly suppressed cross sections, with a suppression of approximately three orders of magnitude over the same mass range. These differences indicate the strong dependence of collider phenomenology on the underlying parameter choices, which highlights the importance of multi-lepton final states as sensitive probes of this model.

For a collider center-of-mass energy of 3 TeV, we assume an integrated luminosity of 1 ab^{-1} [65]. Because this process conserves both charged lepton number and lepton flavor, it receives SM background contributions, with a value 8.19×10^{-4} pb. In order to extract signatures more effectively, we adopt the following criteria [66]:

$$\frac{S}{\sqrt{B+S}} = \frac{\sigma\times\mathscr{L}}{\sqrt{(\sigma_{\rm SM}+\sigma)\times\mathscr{L}}}. \tag{12}$$

The corresponding values are summarized in Table 1, which presents benchmark scenarios B3, B2, and B1 with different combinations of the effective gauge parameters $\tilde{g}/m_{Z'}$ and triplet parameters. For each scenario, we report the predicted signal cross section σ and corresponding statistical significance.

The corresponding cross section can be projected into the plane of $\tilde{g} - m_{Z'}$, as shown in the right panel of Fig. 3. The shaded contours denote the cross sections as functions of the mass $m_{Z'}$ and coupling $\tilde{g}$, with darker regions corresponding to larger signals. Benchmark points B1−B5 are indicated by distinct colored dashed lines, whereas black dashed lines mark the 3σ sensitivity threshold. Among the benchmarks, B1 lies mostly above the 3σ curve for $m_{Z'} > 400$ GeV, thereby indicating strong discovery prospects. In contrast, B2−B5 remain well below the observable threshold. Therefore, the Z' signal could be observable in the high-mass regime at a muon collider under scenario B1. In addition, we check that the triplet scalar has only a minor effect on the overall cross section, which suggests that the gauge sector predominantly determines the collider sensitivity in this channel.

The above analysis is based on an unpolarized case. In practice, the initial-state lepton beams at a muon collider can be polarized in various configurations, as discussed in Refs. [67, 68]. In this study, we considered two representative polarization scenarios: $\{P_{\mu^+}, P_{\mu^-}\}$ = {–20%, 80%} and {80%, –80%}. Under these configurations, the signal significance exhibits notable improvements, as listed in Table 2. For $\{P_{\mu^+}, P_{\mu^-}\}$ = {–20%, 80%}, the significance increases by approximately 14% for benchmark B3 and 11% for B1, relative to the unpolarized case. For $\{P_{\mu^+}, P_{\mu^-}\}$ = {80%, –80%}, the improvement is more substantial —approximately 64% for B3 and 50% for B1.

Table 1. Cross section and statistical significance for different benchmarks at luminosity of $\mathscr{L} = 1\,\text{ab}^{-1}$.

	$(\tilde{g}/m_{Z'})/(10^{-3}\text{GeV}^{-1})$	$m_{Z'}$/GeV	$\tilde{g}$	m_Δ/GeV	Y_{22}	$\sigma\times10^{-4}$/pb	$S/\sqrt{B+S}$
B2	0.25	500	0.125	500	0.25	0.05	0.19
		800	0.20			0.16	0.56
B3	0.3	500	0.15	500	0.05	0.11	0.39
		800	0.24			0.33	1.15
B1	0.62	500	0.31	500	0.415	2.03	6.35
		800	0.496			6.10	16.14

Table 2. Same as Table 1 but for different beam polarization configurations.

	$(\tilde{g}/m_{Z'})$ $/(10^{-3}\text{GeV}^{-1})$	$m_{Z'}$	$\tilde{g}$	m_Δ/GeV	Y_{22}	$\{P_{\mu^+},P_{\mu^-}\}=\{0\%,0\%\}$		$\{P_{\mu^+},P_{\mu^-}\}=\{-20\%,80\%\}$		$\{P_{\mu^+},P_{\mu^-}\}=\{80\%,-80\%\}$	
						$\sigma\times10^{-4}$/pb	$S/\sqrt{B+S}$	$\sigma\times10^{-4}$/pb	$S/\sqrt{B+S}$	$\sigma\times10^{-4}$/pb	$S/\sqrt{B+S}$
B3	0.3	600	0.18	500	0.05	0.18	0.61	0.20	0.7	0.29	1.00
		800	0.24			0.33	1.14	0.38	1.31	0.57	1.88
		1000	0.3			0.49	1.67	0.56	1.91	0.82	2.73
B1	0.62	600	0.36	500	0.415	2.83	8.53	3.23	9.55	4.68	13.05
		800	0.48			5.35	14.53	6.13	16.20	8.90	21.53
		1000	0.6			7.89	19.67	9.01	21.72	14.07	29.82

These enhancements arise because suitable initial-state polarization can suppress background processes that preferentially couple to a specific chirality while simultaneously enhancing the signal cross section. In particular, a large asymmetry between P_{μ^+} and P_{μ^-} maximizes the interference between the SM and Z' amplitudes, thereby boosting the sensitivity in both the cross section and angular observables.

To systematically investigate the implications of our model, we analyze the forward-backward asymmetry $A_{\rm FB}$, which is defined by [69]

$$A_{\rm FB}=\frac{\sigma_F-\sigma_B}{\sigma_F+\sigma_B},\quad \sigma_F=\int_0^1\frac{{\rm d}\sigma}{{\rm d}\cos\theta}{\rm d}\cos\theta,$$
$$\sigma_B=\int_{-1}^0\frac{{\rm d}\sigma}{{\rm d}\cos\theta}{\rm d}\cos\theta. \tag{13}$$

Here, the scattering angle θ is defined as the angle between the outgoing μ and τ in the center-of-mass frame of the collision.

First, we focus on the evolution of the forward-backward asymmetry $A_{\rm FB}$ with respect to the mass $m_{Z'}$, considering the promising benchmark point B1 discussed earlier. By fixing the triplet scalar mass $m_\Delta=500$ GeV, we can isolate the pure impact of the Z' mass on the asymmetry. Within the SM, the process $\mu^+\mu^-\to\mu^\pm\mu^\mp\tau^\pm\tau^\mp$ is governed by γ/Z exchange and yields $A_{\rm FB}^{\rm SM}\sim0$, owing to the absence of chiral flavor violating interference. For $\tilde{g}=0.1$, the allowed region in Fig. 1 corresponds to an $m_{Z'}$ range of 200−1000 GeV. As $m_{Z'}$ increases, the predicted forward-backward asymmetry $A_{\rm FB}$ decreases monotonically and approaches zero at approximately $m_{Z'}\simeq750$ GeV, as shown in Fig. 4. This monotonic decrease reflects the suppression of parity-violating interference effects as Z' becomes heavier. Notably, the transition from positive to negative asymmetry is a characteristic feature of the model and could serve as a discriminating observable in the search for heavy Z' bosons at future colliders. Furthermore, the two curves corresponding to the final states $\mu^-\tau^+$ (blue) and $\mu^+\tau^-$ (red) nearly overlap, corroborating the fact that the forward-backward asymmetry is largely insensitive to the electric charge assignment of the final-state leptons. Note that the behavior of the forward-backward asymmetry in our analysis is a direct consequence of the maximally flavor-violating Z' structure. The maximally flavor-violating scenario in our model arises from the discrete exchange symmetry, $Z'\to-Z'$ and $1\leftrightarrow2$, which is guaranteed even at one-loop level owing to new charge assignment. This exchange symmetry may be broken by quantum corrections at higher loop levels, thereby leading to small flavor-diagonal couplings to muons and taus. However, the resulting flavor-diagonal couplings $\tilde{g}_{\mu\mu}$ are much smaller than the flavor-changing couplings $\tilde{g}_{\mu\tau}$; therefore, the dominant contribution to $A_{\rm FB}$ comes from the flavor-changing couplings, and the corresponding results remain largely unaffected.

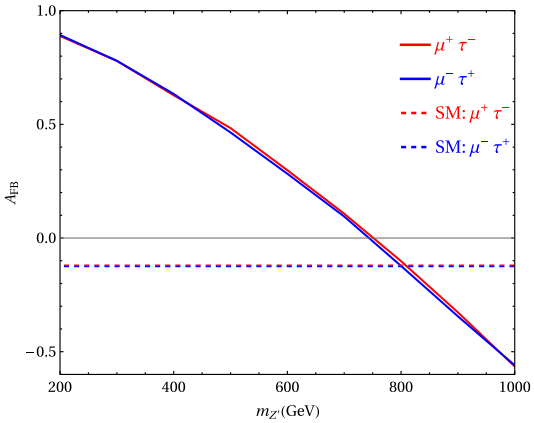

Fig. 4. (color online) Forward-backward asymmetry $A_{\rm FB}$ as a function of $m_{Z'}$ for $\tilde{g}=0.1$ with $m_\Delta=500$ GeV and $Y_{22}=0.415$.

Furthermore, we aim to investigate the individual effects of doubly charged scalars. Because the Z' boson exhibits only vector-current interactions in our model, we can probe the chiral properties of the doubly charged scalars by defining

$$\mathcal{R}=\frac{\sigma_{LR}+\sigma_{LL}-\sigma_{RR}-\sigma_{RL}}{\sigma_{LR}+\sigma_{LL}+\sigma_{RR}+\sigma_{RL}}. \tag{14}$$

Here, σ_{ij}, where $i,j = L,R$, denotes the polarized cross sections, with "L" and "R" denoting 100% left- and right-handed polarizations, respectively. A numerical evaluation yields $\mathcal{R} \simeq -1$, which indicates a maximal left-right asymmetry (100%). This also serves as a cross-check of the interaction structure, where a left-handed vector current (V-A) is mediated by a triplet scalar. To further investigate the details, we similarly analyzed the angular distribution of the differential cross section; the results are shown in Fig. 5. Here, θ is defined as the angle between the two final-state charged leptons originating from the decay of the doubly charged Higgs boson. In the left panel, four different final-state configurations are presented, which reveal that the angular distribution is truncated around $\cos\theta = 0.8$. This is because of the difficulty in distinguishing the final-state μ and τ when the opening angle is small. The structure indicates that $A_{\rm FB}$ tends to be positive, with corresponding values of 0.8772, 0.6216, 0.8736, and 0.622, respectively. In the right panel, the angular distribution is shown for different collider energies, revealing that lower energies correspond to a larger truncation angle in the angular distribution. In addition, when the center-of-mass energy reaches 6 TeV, the angular distribution becomes visible over the full range of $\cos\theta \in [-1,1]$. Although the initial design stage plans to operate at a maximum energy of 3 TeV, a 10 TeV scenario is foreseeable in the future, provided that challenges such as muon beam cooling and short lifetimes of particles are resolved.

In addition to the charged lepton final states, a doubly-charged scalar can decay into a pair of $W^{\pm}$ bosons, with the corresponding expressions as [48]

$$\frac{\Gamma(\Delta^{++} \to W^+W^+)}{\Gamma(\Delta^{++} \to \ell^+\ell^+)} \approx \frac{v_\Delta^2}{v_{\rm SM}^4}\frac{m_\Delta^2}{y^2} \approx 10^{-10}\left(\frac{v_\Delta}{1\ {\rm GeV}}\right)^2\left(\frac{250\ {\rm GeV}}{v_{\rm SM}}\right)^4\left(\frac{m_\Delta/{\rm GeV}}{y}\right)^2, \quad (15)$$

where $v_{\rm SM} = 246$ GeV. We find that the decay into a pair of $W^{\pm}$ primarily depends on the triplet VEV v_Δ, whereas the decay into charged leptons is predominantly governed by the Yukawa coupling. For the $4W$ boson final states originating from $\Delta^{\pm\pm}$ decays, the production cross section with m_Δ is presented in Fig. 6, which explicitly shows the significant role of v_Δ. Furthermore, the cross section exhibits a monotonic increase as m_Δ increases. Additionally, the cross section decreases by several orders of magnitude when decreasing v_Δ from 1 to 10^{-3} (corresponding to red and orange curves, respectively). This behavior is crucial for predicting detectability in collider experiments: higher values of v_Δ and m_Δ increase the cross section to levels potentially observable above background noise.

B. Four-body final states at electron-positron colliders

The muon collider analysis in the previous subsection can also be applied to the case of an electron collider. To facilitate comparison, we chose the same center-of-mass energy $\sqrt{s} = 3$ TeV for the electron-positron collider, as reported in the CILC design [43]. The corresponding integrated luminosity is 3000 fb^{-1}.

Note that, because our model framework involving Z' and $\Delta^{\pm\pm}$ only couples to muons and taus, the electron collider contributes only through s-channel processes to produce $\mu^+\mu^-\tau^+\tau^-$. The corresponding cross sections for four different benchmark points are indicated in the left panel of Fig. 7. A similar increasing trend is observed, consistent with the behavior in Fig. 3. In addition, benchmark B1 yields the largest cross section, approximately $O(10^{-3})$ pb, exceeding those of the other three benchmarks.

For the process $e^+e^- \to \mu^\pm\mu^\mp\tau^\pm\tau^\mp$, the SM background arises from purely γ/Z-mediated processes, 2.92×10^{-5} pb, whereas the signal arises from diagrams involving Z' or doubly charged scalar exchange. Adopting the statistical significance defined in Eq. (12), we can obtain the projected cross section on the plane of $m_{Z'} - \tilde{g}$,

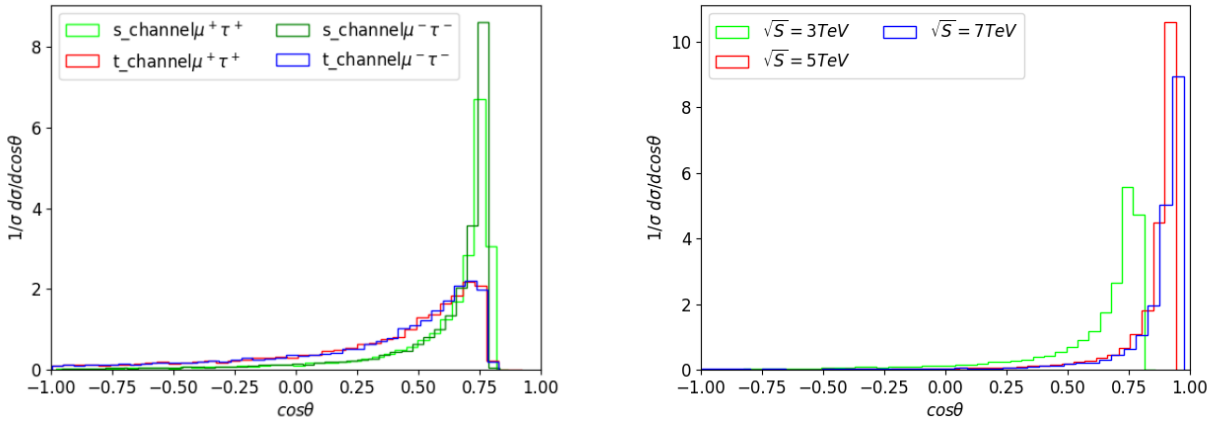

Fig. 5. (color online) (a) Angular distribution at a center-of-mass energy of 3 TeV for different channels. (b) Angular distribution with different collider energies.

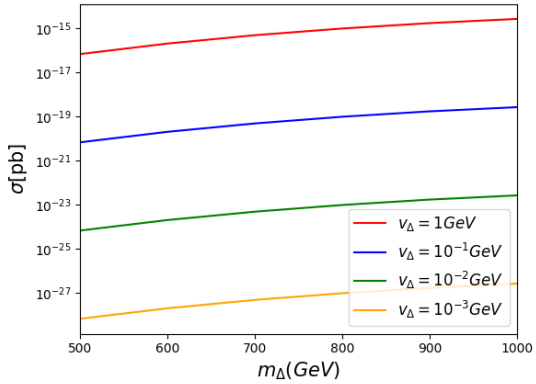

Fig. 6. (color online) Cross section for the process $\mu^+\mu^- \to \Delta^{++}\Delta^- \to 4W$ as a function of mass m_Δ under different values of v_Δ.

as shown in the right panel of Fig. 7. We find that the cross section increases with both $m_{Z'}$ and $\tilde{g}$, reaching a maximum at their largest values. Similarly, four benchmark scenarios (B1−B5) are included for comparison, along with the corresponding 3σ discovery contour. Among these benchmark scenarios, B1 lies well above the 3σ discovery threshold in the entire mass range, thereby indicating the highest potential for an observable signal, consistent with the results from the muon collider case. The only difference compared to the muon collider case is that B2, B3, and B5 can exceed the 3σ discovery threshold at large values of $m_{Z'}$. Specifically, B2 exceeds the threshold when $m_{Z'} \gtrsim 650$ GeV, B3 does so for $m_{Z'} \gtrsim 500$ GeV, and B5 does so for $m_{Z'} \gtrsim 450$ GeV. These results underscore the strong dependence of new physics discovery prospects on the choice of parameter space, particularly in the context of electron collider scenarios.

Similarly, the forward-backward asymmetry was investigated by analyzing the angular distribution, and the results are shown in Fig. 8. A clear trend is observed with increasing mass $m_{Z'}$, which is of great significance for understanding the underlying physical mechanisms and guiding experimental observations.

IV. CONCLUSION

In this study, we investigated the collider phenomenology of a $U(1)_{L_\mu - L_\tau}$ model with maximal flavor violation, concentrating on four-lepton final states as sensitive

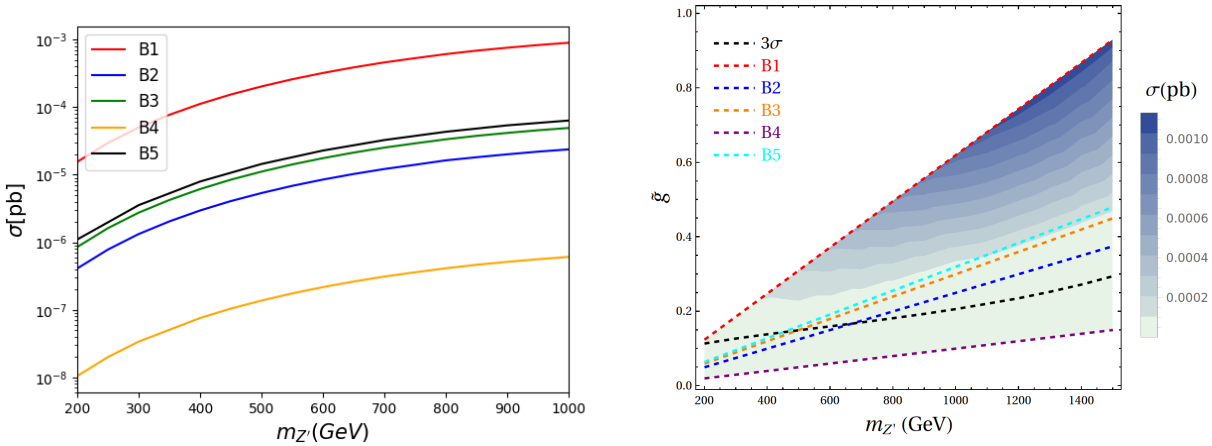

Fig. 7. (color online) Same as Fig. 3 but for $\sigma(e^-e^+ \to \mu^\pm\mu^\mp + \tau^\pm\tau^\mp)$.

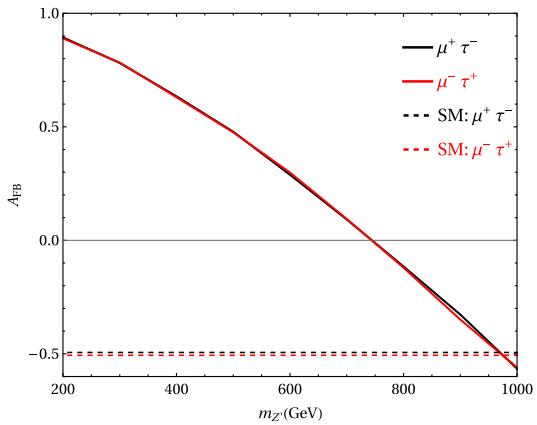

Fig. 8. (color online) Forward-backward asymmetry A_{FB} as a function of $m_{Z'}$ for $\tilde{g} = 0.1$ with $m_\Delta = 500$ GeV and $Y_{22} = 0.415$.

probes of new physics. We showed that the signal cross sections increase with both effective parameters $\tilde{g}/m_{Z'}$ and mass $m_{Z'}$, whereas the contribution from triplet Yukawa couplings remains comparatively small within the phenomenologically allowed regions. We further demonstrated that the forward-backward asymmetry constitutes a robust observable, with its monotonic dependence on $m_{Z'}$ serving as a distinctive signature of the model. Polarization of the initial beams enhances sensitivity by suppressing the SM backgrounds and amplifying the chiral effects associated with the new interactions, thereby facilitating the study of triplet scalar effects. Among the benchmark scenarios considered, the B1 point yields the highest discovery significance, exceeding the 3σ threshold at both muon and electron-positron colliders. The B2 and B3 scenarios also offer good sensitivity at electron colliders for large values of $m_{Z'}$. The difference between electron and muon colliders lies in the presence of additional t- and u-channel contributions in the muon collider, in contrast to the electron collider, which only involves s-channel processes.

Overall, our study showed that high-energy lepton colliders can offer clear and testable signatures of the $U(1)_{L_\mu - L_\tau}$ framework. Multi-lepton final states, in conjunction with polarization and angular observables, provide experimentally accessible handles to probe lepton flavor violation and to explore the underlying gauge and scalar dynamics of the model.

References

[1] J. L. Rosner, arXiv: hep-ph/0108195
[2] L. Calibbi and G. Signorelli, Riv. Nuovo Cim. **41**(2), 71 (2018), arXiv: 1709.00294[hep-ph]
[3] S. Jahedi, Y. Liao, and X. D. Ma, arXiv: 2507.13876[hep-ph]
[4] M. Hirsch, S. Kaneko, and W. Porod, Phys. Rev. D **78**, 093004 (2008), arXiv: 0806.3361[hep-ph]
[5] Y. K. Huang, J. L. Yang, S. K. Cui *et al.*, Phys. Rev. D **110**(7), 075040 (2024), arXiv: 2409.16628[hep-ph]
[6] S. P. Das, F. F. Deppisch, O. Kittel *et al.*, Phys. Rev. D **86**, 055006 (2012), arXiv: 1206.0256[hep-ph]
[7] J. Barry and W. Rodejohann, JHEP **09**, 153 (2013), arXiv: 1303.6324[hep-ph]
[8] F. F. Deppisch, T. E. Gonzalo, S. Patra *et al.*, Phys. Rev. D **91**(1), 015018 (2015), arXiv: 1410.6427[hep-ph]
[9] G. Bambhaniya, P. S. B. Dev, S. Goswami *et al.*, JHEP **04**, 046 (2016), arXiv: 1512.00440[hep-ph]
[10] C. Bonilla, M. E. Krauss, T. Opferkuch *et al.*, JHEP **03**, 027 (2017), arXiv: 1611.07025[hep-ph]
[11] D. Chowdhury and K. M. Patel, Phys. Rev. D **87**(9), 095018 (2013), arXiv: 1304.7888[hep-ph]
[12] X. G. He, C. J. Lee, J. Tandean *et al.*, Phys. Rev. D **91**(7), 076008 (2015), arXiv: 1411.6612[hep-ph]
[13] P. S. Bhupal Dev and Y. Zhang, JHEP **10**, 199 (2018), arXiv: 1808.00943[hep-ph]
[14] A. Crivellin, F. Kirk, and C. A. Manzari, JHEP **12**, 031 (2022), arXiv: 2208.00020[hep-ph]
[15] S. Davidson, D. C. Bailey, and B. A. Campbell, Z. Phys. C **61**, 613 (1994), arXiv: hep-ph/9309310
[16] I. Doršner, S. Fajfer, A. Greljo *et al.*, Phys. Rept. **641**, 1 (2016), arXiv: 1603.04993[hep-ph]
[17] I. d. Varzielas and A. Sengupta, Nucl. Phys. B **1001**, 116495 (2024), arXiv: 2301.04119[hep-ph]
[18] B. De, Phys. Lett. B **855**, 138784 (2024), arXiv: 2405.06970 [hep-ph]
[19] Y. Cheng, C. W. Chiang, X. G. He *et al.*, Phys. Rev. D **104**(1), 013001 (2021), arXiv: 2012.15287[hep-ph]
[20] J. Sun, Y. Cheng, and X. G. He, JHEP **04**, 141 (2021), arXiv: 2101.06055[hep-ph]
[21] R. Foot, X. G. He, H. Lew *et al.*, Phys. Rev. D **50**, 4571 (1994), arXiv: hep-ph/9401250
[22] J. Y. Cen, Y. Cheng, X. G. He *et al.*, Nucl. Phys. B **978**, 115762 (2022), arXiv: 2104.05006[hep-ph]
[23] Y. Cheng, X. G. He, and J. Sun, Phys. Lett. B **827**, 136989 (2022), arXiv: 2112.09920[hep-ph]
[24] F. Huang and J. Sun, Phys. Rev. D **110**(11), 115047 (2024), arXiv: 2409.13249[hep-ph]
[25] J. Liu, M. Song, and H. Zhang, JHEP **10**, 128 (2024), arXiv: 2407.05831[hep-ph]
[26] X. G. He, G. C. Joshi, H. Lew *et al.*, Phys. Rev. D **43**, 22 (1991)
[27] X. G. He, G. C. Joshi, H. Lew *et al.*, Phys. Rev. D **44**, 2118 (1991)
[28] W. Rodejohann and M. A. Schmidt, Phys. Atom. Nucl. **69**, 1833 (2006), arXiv: hep-ph/0507300
[29] J. Heeck and W. Rodejohann, Phys. Rev. D **84**, 075007 (2011), arXiv: 1107.5238[hep-ph]
[30] K. Asai, K. Hamaguchi, N. Nagata *et al.*, Phys. Rev. D **99**(5), 055029 (2019), arXiv: 1811.07571[hep-ph]
[31] C. Majumdar, S. Patra, P. Pritimita *et al.*, JHEP **09**, 010 (2020), arXiv: 2004.14259[hep-ph]
[32] J. Heeck and A. Thapa, Eur. Phys. J. C **82**(5), 480 (2022), arXiv: 2202.08854[hep-ph]
[33] X. g. He, arXiv: hep-ph/9409237
[34] G. Aad *et al.* (ATLAS), JHEP **23**, 082 (2020), arXiv: 2307.08567[hep-ex]
[35] W. Porod and W. Majerotto, Phys. Rev. D **66**, 015003 (2002), arXiv: hep-ph/0201284
[36] T. Li and M. A. Schmidt, Phys. Rev. D **99**(5), 055038 (2019), arXiv: 1809.07924[hep-ph]
[37] P. S. B. Dev, R. N. Mohapatra, and Y. Zhang, Phys. Rev. Lett. **120**(22), 221804 (2018), arXiv: 1711.08430[hep-ph]
[38] Q. Qin, Q. Li, C. D. Lü *et al.*, Eur. Phys. J. C **78**(10), 835 (2018), arXiv: 1711.07243[hep-ph]
[39] K. Fridell, R. Kitano, and R. Takai, JHEP **06**, 086 (2023), arXiv: 2304.14020[hep-ph]
[40] J. Sun, F. Huang, and X. G. He, Phys. Lett. B **845**, 138121 (2023)
[41] W. Altmannshofer, P. Munbodh, and T. Oh, JHEP **08**, 026 (2023), arXiv: 2305.03869[hep-ph]
[42] J. Li and Z. You, PoS ICHEP **2024**, 447 (2025)
[43] M. Aicheler *et al.* (CLIC accelerator), Doi: 10.23731/CYRM-2018-004, arXiv: 1903.08655 [physics.acc-ph]
[44] T. Barklow, J. Brau, K. Fujii *et al.*, arXiv: 1506.07830 [hep-ex]
[45] W. Abdallah *et al.* (CEPC Study Group), Radiat. Detect.

Technol. Methods **8**(1), 1 (2024) [Erratum: Radiat. Detect. Technol. Methods **9**(1), 184 (2025)], arXiv: 2312.14363 [physics.acc-ph]
[46] X. Ai, W. Altmannshofer, P. Athron *et al*., Chin. Phys. **49**(10), 103003 (2025), arXiv: 2412.19743[hep-ex]
[47] A. Abada *et al*. (FCC), Eur. Phys. J. ST **228**(2), 261 (2019)
[48] F. Huang and J. Sun, Phys. Lett. B **872**, 140047 (2026), arXiv: 2507.04614[hep-ph]
[49] J. de Blas *et al.* (Muon Collider), arXiv: 2203.07261 [hep-ph]
[50] G. Lazarides, Q. Shafi, and C. Wetterich, Nucl. Phys. B **181**, 287 (1981)
[51] R. N. Mohapatra and G. Senjanovic, Phys. Rev. D **23**, 165 (1981)
[52] W. Konetschny and W. Kummer, Phys. Lett. B **70**, 433 (1977)
[53] T. P. Cheng and L. F. Li, Phys. Rev. D **22**, 2860 (1980)
[54] M. Magg and C. Wetterich, Phys. Lett. B **94**, 61 (1980)
[55] J. Schechter and J. W. F. Valle, Phys. Rev. D **22**, 2227 (1980)
[56] S. Ashanujjaman and K. Ghosh, JHEP **03**, 195 (2022), arXiv: 2108.10952[hep-ph]
[57] D. P. Aguillard *et al*. (Muon g-2), Phys. Rev. Lett. **135**(10), 101802 (2025), arXiv: 2506.03069[hep-ex]
[58] R. Aliberti, T. Aoyama, E. Balzani *et al*., Phys. Rept. **1143**, 1 (2025), arXiv: 2505.21476[hep-ph]
[59] A. Pich, I. Boyko, D. Dedovich *et al*., Int. J. Mod. Phys. A 24S **1**, 715 (2009)
[60] Y. S. Amhis *et al*. (HFLAV), Phys. Rev. D **107**(5), 052008 (2023), arXiv: 2206.07501[hep-ex]
[61] L. Corona (Belle-II), arXiv: 2405.09974 [hep-ex]
[62] D. Geiregat *et al*. (CHARM-II), Phys. Lett. B **245**, 271 (1990)
[63] S. R. Mishra *et al*. (CCFR), Phys. Rev. Lett. **66**, 3117 (1991)
[64] T. Adams *et al*. (NuTeV), Phys. Rev. D **61**, 092001 (2000), arXiv: hep-ph/9909041
[65] C. Aime, A. Apyan, M. A. M. Mohammed *et al.*, arXiv: 2203.07256 [hep-ph]
[66] G. Cowan, K. Cranmer, E. Gross and O. Vitells, Eur. Phys. J. C **71**, 1554 (2011) [Erratum: Eur. Phys. J. C **73**, 2501 (2013)], arXiv: 1007.1727[physics.data-an]
[67] S. Aiola *et al.* (CMB-HD), arXiv: hep-ph/2203.05728
[68] C. Chen, X. Mo, M. Selvaggi *et al*., arXiv: 1712.09517 [hep-ex]
[69] S. Schael *et al*. (ALEPH, DELPHI, L3, OPAL, SLD, LEP Electroweak Working Group, SLD Electroweak Group and SLD Heavy Flavour Group), Phys. Rept. **427**, 257 (2006), arXiv: hep-ph/0509008